Global Solar Energy, Inc.
5575 South Houghton Road
Tucson, Arizona 85747
(520) 546-6313 (Voice)
(520) 546-6318 (FAX)

November 24, 2003

Dr. Harin Ullal
Mail Stop 3212
National Renewable Energy Laboratory
1617 Cole Blvd
Golden, CO 80401-3393

Re: Phase II, Second Quarterly Report #ZDJ-2-30630-14

Dear Harin,

This letter comprises the quarterly technical status report for Thin Film Partnership subcontract # ZDJ-2-30630-14. The reported work was performed during the second quarter of year 2 for this contract, from 8/15/03 to 11/15/03. This report describes activities performed by GSE, as well as those performed by lower-tier subcontractor ITN Energy Systems, Inc.

INTRODUCTION

Two-stage and three-stage CIGS coevaporation – followed by chemical bath CdS and RF-sputtered resistive and conductive ZnO – have come to be viewed as laboratory standards for the deposition of CIGS photovoltaic devices. However, a number of conditions are encountered during continuous manufacturing that prevent an exact replication of the laboratory processes. Such differences include both those imposed by continuous processing of moving substrates, and those implemented to decrease costs and increase throughput. It is, therefore, beneficial to understand the tolerance of the established laboratory processes to variations in deposition procedures.

Research under this program consists of four basic parts to examine the tolerance of the established laboratory process to variations in deposition procedures:

1. Setting up the National Renewable Energy Laboratory (NREL)-developed three-stage CIGS laboratory process in a bell jar.

2. Characterizing the GSE roll-to-roll production chambers and device finishing steps in terms of the variables important to the laboratory processes.

3. Using the bell jar system to step incrementally from the NREL process to the conditions experienced by a sample during manufacturing, and characterizing the resulting films and devices.

4. Applying the process sensitivity information gained from the bell jar system to the production systems.

Some portions of these tasks are being performed in parallel. This quarter, activities related to maximum Cu ratio during CIGS growth, temperature during CIGS growth, roll-coater metals flux profiles, and window layer sensitivities.

MAXIMUM CU RATIO DURING CIGS GROWTH

Impact on Bell Jar Devices

CIGS deposition temperatures were varied in the bell jar to assess the impact of straying from process setpoints on device performance. During this examination, it was discovered that unintentional variations in maximum Cu ratio (i.e. the atomic ratio Cu/group III at the end of the second stage) had a stronger effect on device efficiency than the intentional temperature variations. Specifically, it was found that

- For devices with low final Cu ratio ($R_3 \leq 0.9$), device efficiency improves continuously with maximum Cu ratio approaching 1.15.

- By the time maximum Cu ratio reaches 1.3, a significant decrease in efficiency is observed.

- Efficiency falls off as final Cu ratio approaches 1, but some samples tolerate a higher final Cu ratio than others.

- The controlling condition for limit on maximum final Cu ratio is not apparent from the present data.

The importance of a Cu-rich growth period has been the subject of some disagreement in the literature, with various studies confirming its importance,[1,2,3,4] and others finding it important only under specialized circumstances.[5,6,7] Since the Cu-rich period enhances growth kinetics via existence of liquid copper selenide, it is therefore surmised that Cu-rich growth is most important in situations where grain growth encounters other unfavorable conditions, such as fast deposition rates, low temperatures, or unoptimized supply of Na. Thus, the bell jar findings described in the paragraphs below are currently being revisited using Ga content and deposition rates as similar as possible to those in the roll-coaters.

[1] D. S. Albin, G.D. Mooney, A. Duda, J. Tuttle, R. Matson, R. Noufi, *Solar Cells* **30**, 47, (1991).

[2] A.M. Gabor, J.R. Tuttle, D.S. Albin, M.A. Contreras, R. Noufi, A.M. Herman, "High-efficiency $CuIn_xGa_{1-x}Se_2$ solar cells made from $(In_x,Ga_{1-x})_2Se_3$ precursor films", *Applied Physics Letters*, **65**(2), (1994), pp. 198-200.

[3] B. M. Keyes, P. Dippo, W. Metzger, J. AbuShama, R. Noufi, "$Cu(In,Ga)Se_2$ Thin Film Evolution During Growth – A Photoluminescence Study", *Conference Record of the Twenty-Ninth IEEE Photovoltaics Specialists Conference*, (2002).

[4] J.R. Tuttle, J.R. Sites, A. Delahoy, W. Shafarman, B. Basol, F. Fonash, J. Gray, R. Menner, J. Phillips, A. Rockett, J. Scofield, F.R. Shapiro, P. Singh, V. Suntharalingam, D. Tarrant, T. Walter, S. Wiedeman, T.M. Peterson, "Characterization and Modeling of $Cu(In,Ga)(S,Se)_2$-based Photovoltaic Devices: A Laboratory and Industrial Perspective," *Progress in Photovoltaics: Research and Applications*, **3**, pp. 89-104, (1995).

[5] W.N. Shafarman, R.W. Birkmire, S. Marsillac, M. Marudachalam, N. Orbey, T.W.F Russell, "Effect of Reduced Deposition Temperature, Time, and Thickness, on $Cu(In,Ga)Se_2$ Films and Devices", *Conference Record of the 25th IEEE Photovoltaic Specialists Conference*, (1996), pp.331-334.

[6] W.N. Shafarman, J. Zhu, "Effect of Substrate Temperature and Deposition Profile on Evaporated $Cu(In,Ga)Se_2$ films and devices", *Thin Solid Films* **361-362**, (2000), pp. 473-477.

[7] S. Nishiwaki, T. Satoh, S. Hayashi, Y. Hashimoto, T. Negami, T. Wada, "Preparation of $Cu(In,Ga)Se_2$ thin films from In-Ga-Se precursors for high-efficiency solar cells", *Journal of Materials Research* **14** (12) , (1999), pp. 4514-4520.

Device parameters were analyzed as a function of maximum and final Cu ratio for 75 devices on 25 substrates. As the 25 substrates were taken from studies involving intentional variations in temperature, venting, and cool-down procedures, such variations are expected to add some scatter to the Cu-ratio analysis. However, it is apparent that the intentional variables are not the strongest influence on device efficiency. For each 3" ×3" substrate, several pieces of information were tabulated. Grids were oriented relative to position in the chamber. Device results at the center, the Ga boat front corner (most Cu rich), and the In boat back corner (most Cu-poor) were recorded. Each of these device results were associated with a final Cu ratio, based on the XRF measurement at the film center, and on earlier examinations of Cu ratio nonuniformity. It was estimated that the Cu ratio for the Ga front corner device is 5% larger than that of the center device, and the Cu ratio for the In back corner device is 5% smaller than that of the center device. Next, logged flux profiles were used to convert each final Cu ratio ("R_3") to a maximum Cu ratio ("R_2"). Assuming a constant group III deposition rate in stages 1 and 3, the maximum Cu ratio for any device is

$$R_2 = R_3 \times \text{(stage 1 + stage 3 deposition time)/(stage 1 deposition time)} \qquad (i)$$

Two major trends are apparent. First, for devices with low final Cu ratio ($R_3 \leq 0.9$), device efficiency improves continuously with maximum Cu ratio approaching 1.15. These data are shown in Figure 1. Points from the same substrate are connected by lines. Some points in Figure 1 are not connected in a set of three, as the other devices on the substrates either did not satisfy the condition $R_3 \leq 0.9$, or were shunted. (Devices are deduced to be shunted by localized defects if fill factor is less than 40%, and efficiency at least 2% less than the neighboring device.) 10% devices were only produced with maximum Cu ratio exceeding 1, and 11%+ devices were only produced with maximum Cu ratio exceeding 1.05. Efficiency loss for lower Cu ratios is spread comparably over V_{oc}, and fill factor. Device parameters for the efficiency data of Figure 1 are shown in Figure 2.
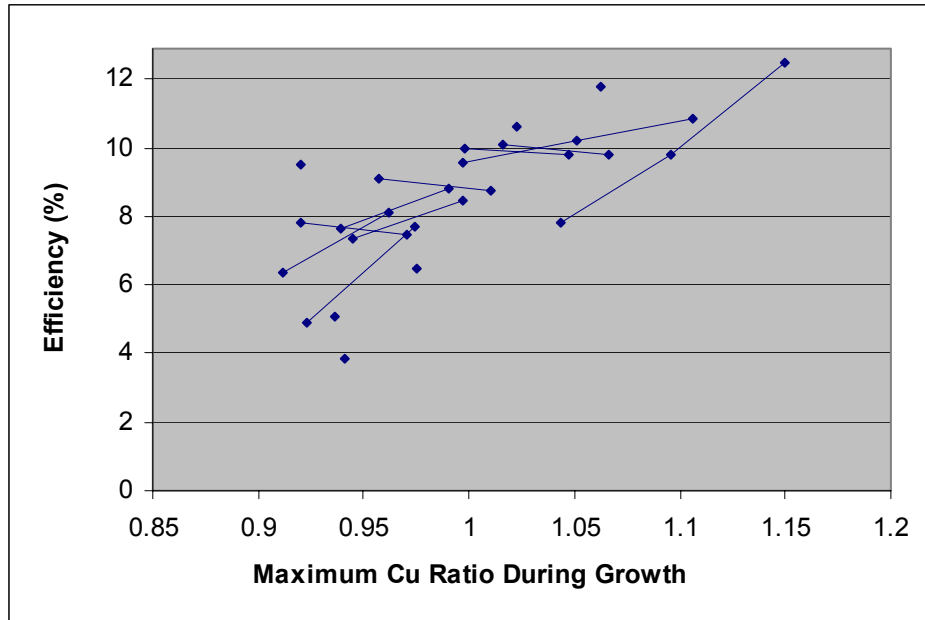

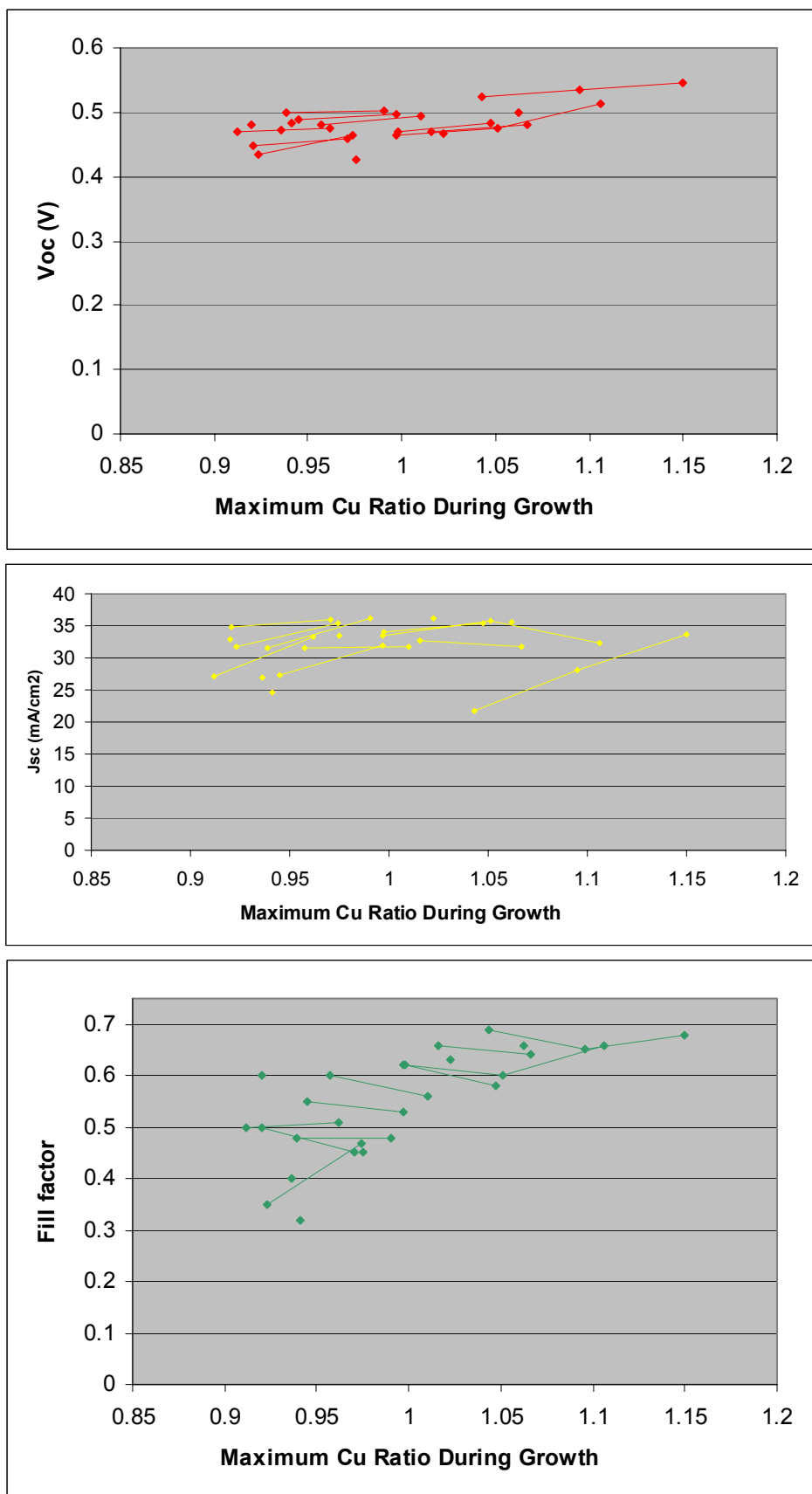Figure 1: Efficiency as a function of maximum Cu ratio for devices with final Cu ratio ≤ 0.9.

Figure 2: Device parameters for efficiency data shown in previous figure.

The second trend apparent in the data is that efficiency falls off as final Cu ratio approaches 1, but some samples tolerate a higher final Cu ratio than others. Figure 3 shows efficiency as a function of final Cu ratio for all samples in the study. At present it is unclear whether tolerance of a high final Cu ratio is a function of the maximum Cu ratio, or other variables in the study, such as temperature. Given that there seems to be no efficiency penalty for final Cu ratios in the range 0.8 to 0.9 (based on this and other[8] studies), it is currently recommended that CIGS films be produced with a final Cu ratio less than or equal to 0.9.
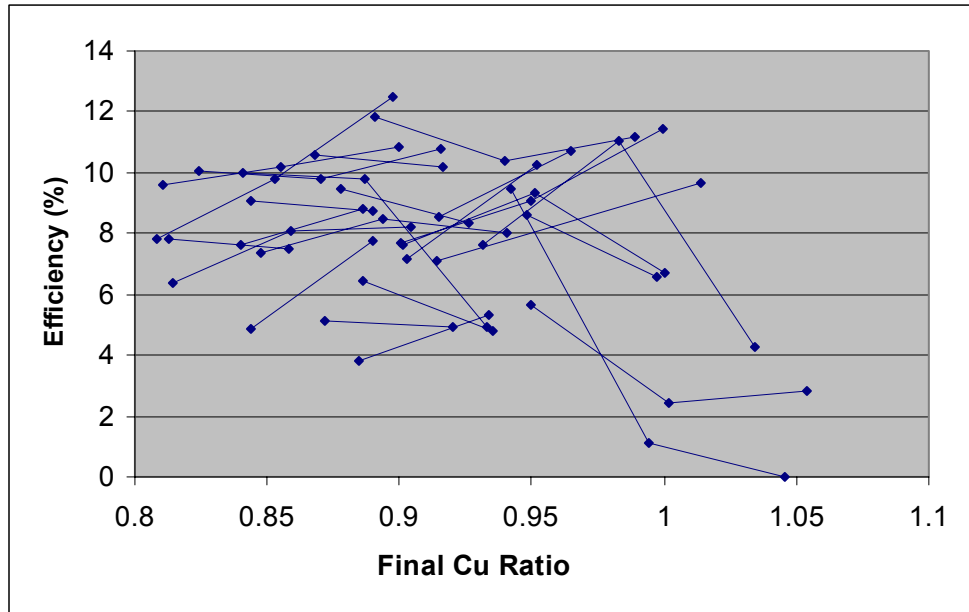

Figure 3: Efficiency as a function of final Cu ratio for all devices in study.

After the above trends in efficiency were recognized, four CIGS depositions were performed to determine an acceptable processing window for maximum Cu ratio. Devices with maximum Cu ratios (i.e. Cu ratio at the end of stage 2) between 1.2 and 1.4 exhibited low open-circuit voltages, and efficiencies near 5%.

X-axis uncertainty in Figure 1 and related graphs is considerable. The final composition of the film center is repeatable to within ±1% , due to noise in the XRF. Furthermore, the Cu ratio gradient across the sample may change slightly from run to run, due to boat positioning, film Ga content, and grid registration. Thus, the final composition ratio of the corner devices carries and additional approximate ±2% uncertainty. Deduction of maximum Cu ratio from final Cu ratio introduces further uncertainty.   Use of equation (i) assumes constant group III deposition rates throughout stage 1 and 3. In some instances, this assumption is clearly not valid. For example, in some depositions, the Ga rate in stage 3 reaches its setpoint prior to the In rate. Thus, if the In deposition time is used as the stage 3 time, the maximum Cu ratio is underestimated. Furthermore, it is possible that drift in the EIES calibration – perhaps a function of temperature or Se pressure – occurs over the course of the deposition.

---

[8] A.M. Gabor, J.R. Tuttle, D.S. Albin, M.A. Contreras, R. Noufi, A.M. Herman, "High-efficiency $CuIn_xGa_{1-x}Se_2$ solar cells made from $(In_x,Ga_{1-x})_2Se_3$ precursor films", *Applied Physics Letters*, **65**(2), (1994), pp. 198-200.

Monitoring Maximum Cu Ratio in Production Roll Coaters

It was described in the Phase I annual report that a novel non-contact method to control the Cu-rich growth excursion has been developed in the bell jar. IR monitoring of the substrate was found to provide unambiguous detection of the Cu-poor to Cu-rich transition, as well as the transition back from Cu-rich to Cu-poor. To date, the sensor has provided non-contact control of the Cu-rich excursion over approximately one hundred CIGS depositions in the bell jar. Work to determine if this IR monitoring method can be applied to the production systems is underway. Both hardware and analytical challenges exist. First, the production systems will expose the sensor body to more heat than the bell jar. Second, in the production system, information must be interpreted in a continuous mode, as the sensor sees one portion of the process over and over, rather than seeing all stages consecutively.

The issue of sensor heating in the production environment was attacked this quarter. The IR sensor was installed in a production roll-coater, initially in a post-deposition zone for testing. Although composition in the roll-coaters is measured by in-situ x-ray fluorescence installed just after the deposition zone, the IR sensor has potential advantages. It is likely that the IR sensor can be installed between the second and third deposition stages due to its compact size, narrow field of view, and potential to withstand elevated temperatures. It is also a low-cost sensor.

Results from the initial tests were mixed. As expected, the IR sensor did show an increase in signal for Cu ratios exceeding one. Figure 4 shows an example of composition and IR sensor data from the roll-coater. The system was perturbed at 6500 seconds to verify that when Cu ratio exceeds one (in green), the signal from the IR sensor (in red) increases. However, the signal increase is a smaller fraction of the total signal than when the sensor is used in the bell jar, most likely due to the elevated operating temperature in the roll-coater. Furthermore, after approximately 50 hours of deposition, the IR sensor failed due to disintegration of the optics. Thus, the sensor was subsequently fitted with higher temperature optics and thermally stressed in a series of furnace bakes. The modified sensor survived thermal testing, and installation between deposition stages two and three in the roll-coater is currently underway.
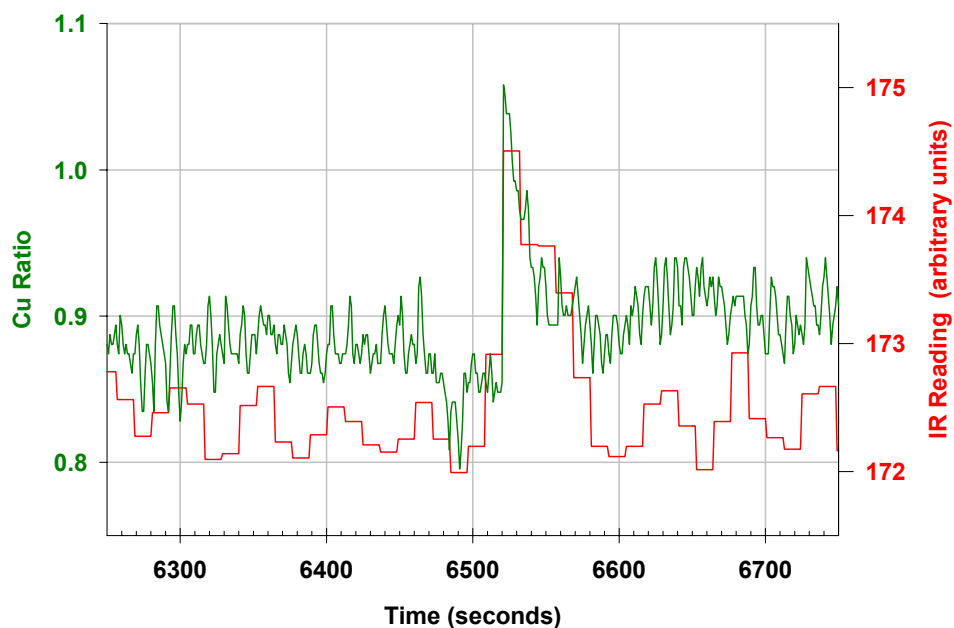

Figure 4: Example of data from initial IR sensor tests in production roll-coater.

6

CIGS DEPOSITION TEMPERATURE

As mentioned in the previous section, device performance variations seen during a study of temperature variations were actually dominated by the maximum Cu ratio during growth. When temperature differences are noted on the data from Figure 1, the data appear as shown in Figure 5. Here, devices fabricated at the same temperatures are shown in the same colors. The red line shows a second-order least-squares fit to all the data, which can be used to account for the effect of maximum Cu ratio. Devices above the red line are more efficient than average, and devices below the red line are less efficient than average. Figure 6 shows, for each first stage temperature, the average distance the data points fall above the red fit line. No trend is apparent.
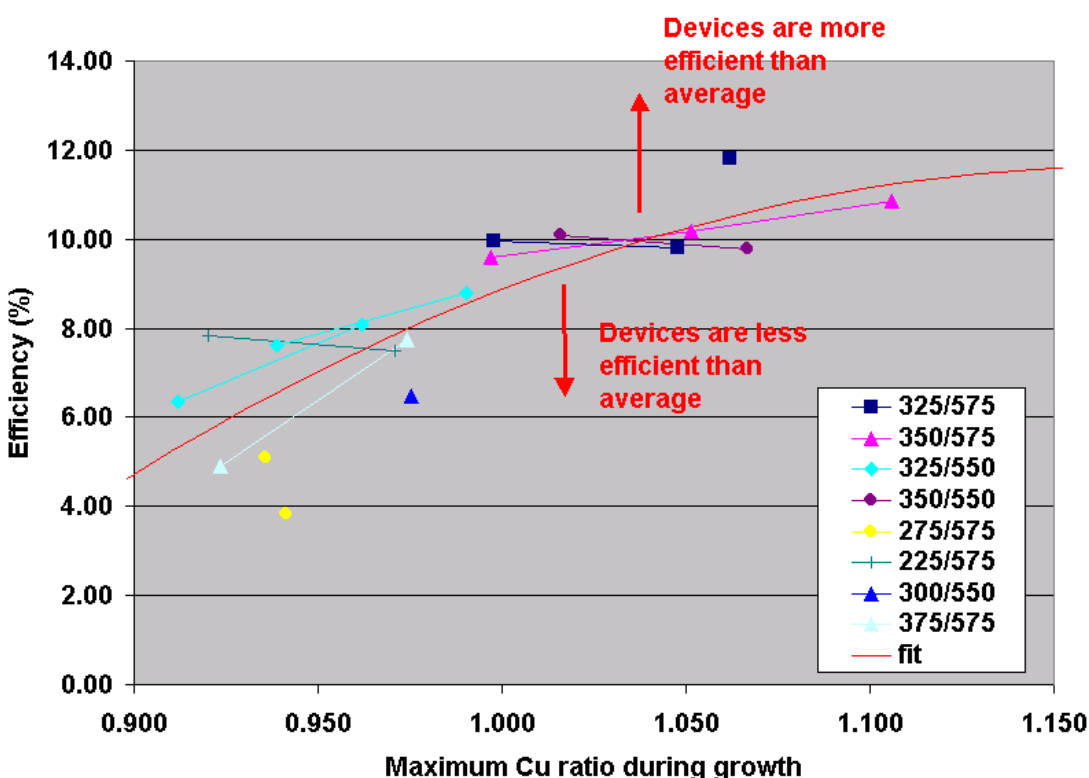

Figure 5: Efficiency as a function of maximum Cu ratio and temperature for devices with final Cu ratio < 0.9.
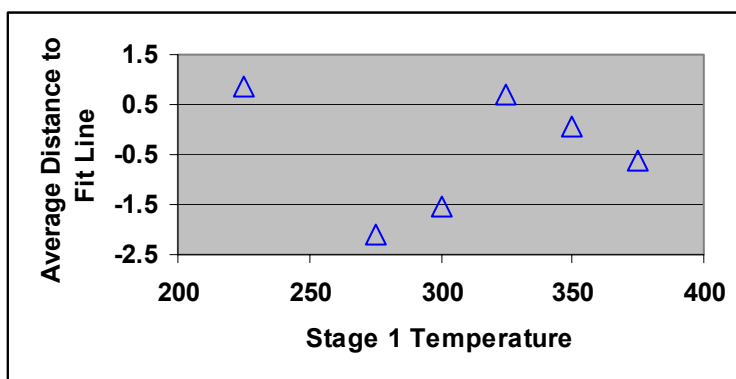

Figure 6: Efficiency variation, corrected for maximum Cu ratio, as a function of stage 1 temperature.

In Figure 5 and related data, some variability in device performance is evident beyond what can be attributed to variations in maximum Cu ratio or temperature. Similar (2-3%) variability is a common attribute of data published by laboratory groups. Reducing the variability below 0.5% in efficiency is desirable, both to gain understanding of important factors to be controlled during production, and to lessen the number of experiments that must be performed to quantify the impact of a given process variation. Several activities are currently underway to better understand and minimize variability. First, software is being developed to automatically identify the Cu-rich emissivity change and to insure that maximum and final Cu-ratios are very consistent and operator-independent. Second, the reproducibility and overall quality of window layers and substrates are also being assessed. Third, an examination of the effect of venting and sample cool-down procedures on device performance is underway.

ROLL-COATER METALS FLUX PROFILES

Last quarter, flux as a function of position was characterized for the production evaporation sources, as described in the previous report. This quarter, CIGS depositions were performed in the bell jar using flux vs. time profiles that imitate those expected in the roll-coaters. This progression is illustrated in Figure 7. Figure 7a shows the flux as a function of position (or equivalently time, for the moving production substrate) from a roll-coater Cu source, as reported last quarter. Figure 7b shows the standard three-stage flux profiles used in the bell jar at ITN. Figure 7c shows the three-stage flux profiles modified to deposit a film of similar composition and thickness, while imitating the flux vs. time seen by a substrate in the roll-coater. The flux profiles of Figure 7c were created by varying with time the setpoint assigned to the electron impact emission spectrometer rate controller.

The insets in Figure 7b and Figure 7c show efficiencies for devices made using each type of flux profile. The listed device parameters describe the highest total-area efficiency 1 cm^2 device on each 3" × 3" substrate. No AR coating was applied to these devices. Work is currently underway to separate and quantify the impacts of deposition rate, instantaneous Se to metals ratio, and variability on the results. The listed results should be viewed as preliminary until the underlying causes are better defined. Furthermore, the flux profiles of Figure 7 should be combined with roll-coater substrate temperature profiles to best simulate then optimize absorber formation in the roll-coaters.

WINDOW LAYER SENSITIVITIES

Time Between CIGS and CdS

Sensitivity of device performance to air exposure time between CIGS and CdS processing was examined. Long exposure times were examined using the production systems at GSE, while very short exposure times were examined using the bell jar at ITN. Data from the production systems are shown in Figure 8, where each position corresponds to 200 individual devices randomized over 20 sq. ft. of substrate/absorber. Post CdS window layer completion was performed simultaneously for all devices. Squares indicate the mean value of each device parameter as a function of air exposure time. Error bars indicate ±95% confidence intervals based on the distribution of devices made under one condition. Slight downward trends in
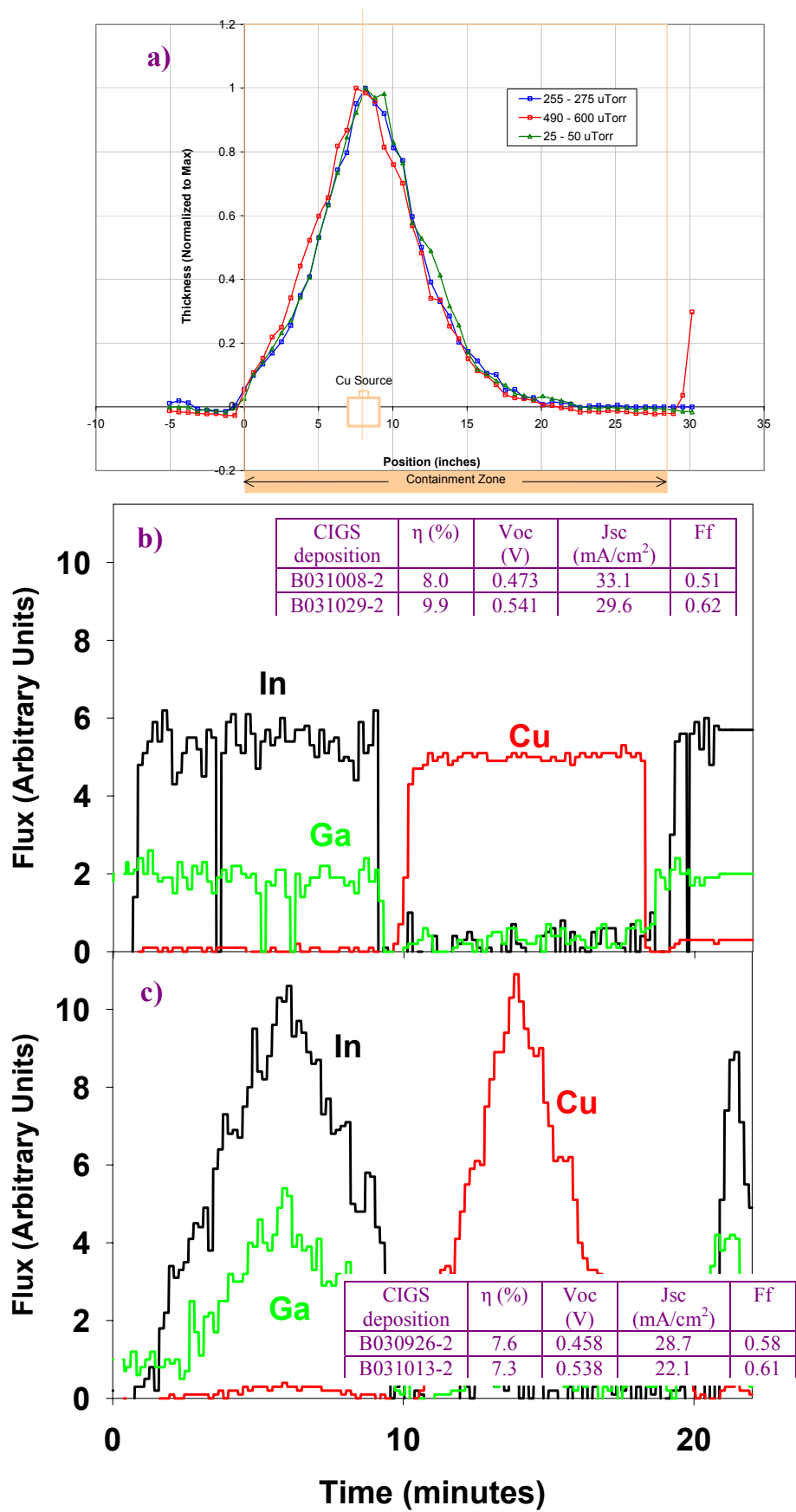
Figure 7: *Flux profile a) measured in roll-coater, b) used in bell jar for standard three stage recipe, and c) used in bell jar to imitate roll-coater.*

efficiency and fill factor with increasing air exposure time are evident. It should be noted that although plotted on a linear scale, the air exposure time scale (x-axis) is not linear According to these results, longest times explored should therefore be avoided when scheduling processing steps.
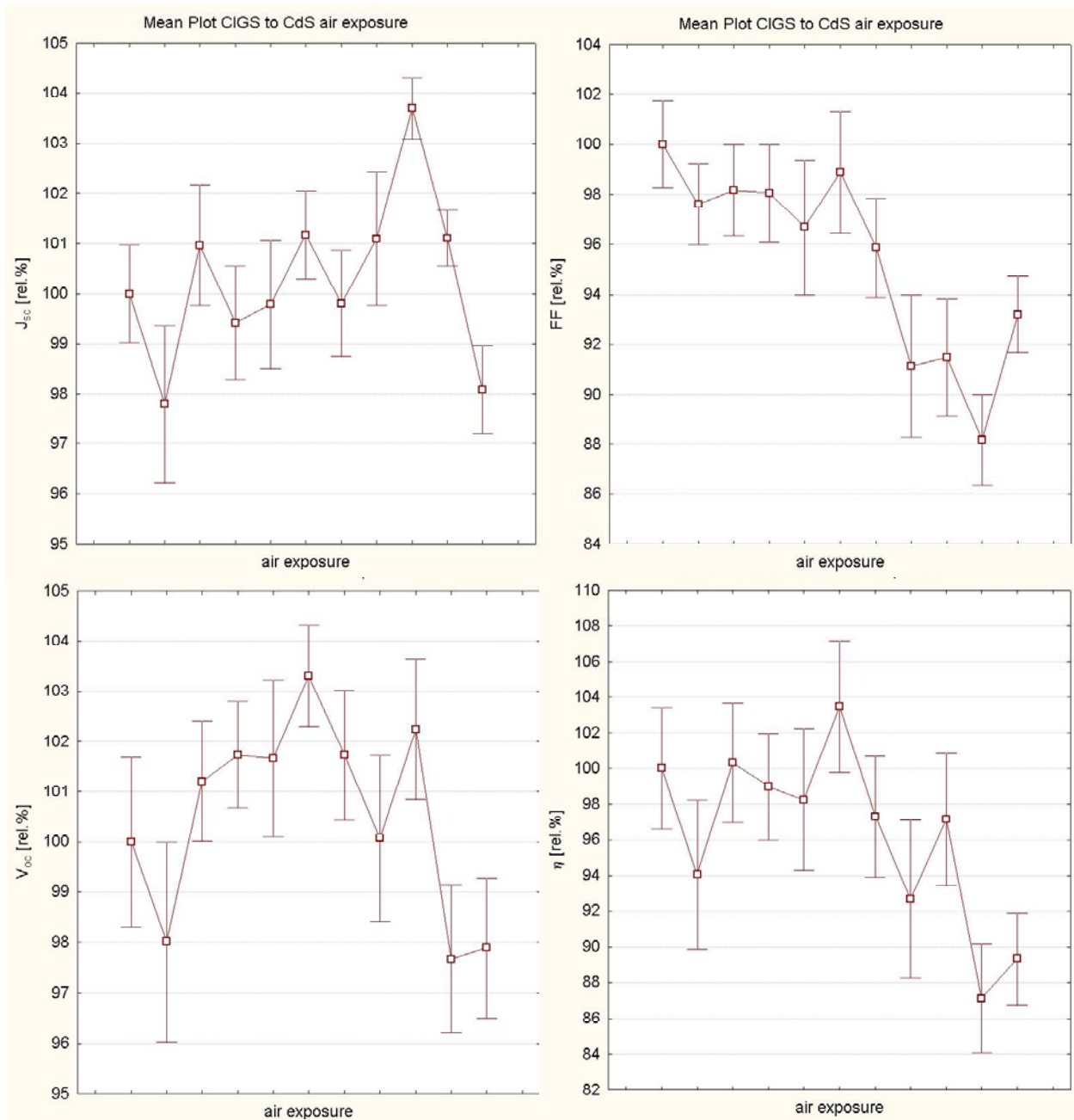

Figure 8: Device parameters as a function of air exposure time between CIGS and CdS processing.

Using the bell jar at ITN, air exposure times shorter than those currently practical on the production floor were examined. Each sample in the study was deposited using standard three-stage conditions. Upon venting, the sample was quickly removed from the chamber and cut in half in the direction perpendicular to composition gradients. The "rushed half" was immersed in the waiting CdS bath within three minutes of first air exposure, while – for maximum contrast – the "delayed" half was stored in air for two weeks before receiving CdS. JV characteristics for

two such trials are shown in Figure 9. For sample #1, the rushed CdS half shows the JV curve inflection that has been associated with band offsets or interface states acting as a barrier at the CdS/CIGS interface (black curve).[9],[10] Furthermore, the rushed CdS sample is not stable. A second measurement, taken three weeks later (green curve), is markedly different. The delayed half of the sample (red and yellow curves) shows no such effects. For sample #2, the rushed half (blue curve) exhibited standard behavior, suggesting that the effect of reducing air exposure time is very sensitive either to ambient conditions (such as humidity) or to CIGS properties – e.g., degree of In and Ga at the surface, associated oxide formation, and subsequent bath chemistry interactions.[11] In any case, no efficiency gain was realized by shortening the time between venting and CdS. Furthermore, in one case, metastability and decreased efficiency were associated with the decreased time.
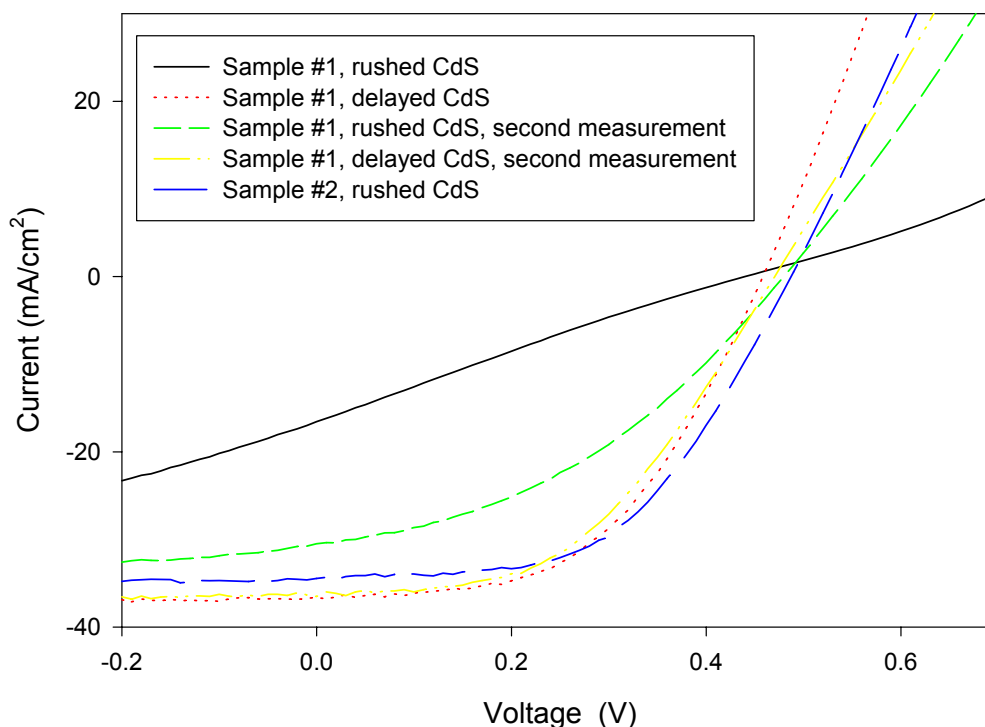

Figure 9: Current-voltage characteristics of baseline CIGS with rushed or delayed CdS.

Stability of Transparent Conducting Oxide

In a joint study with the National Renewable Energy Laboratory (NREL) and the Institute for Energy conversion (IEC), the effects of damp heat exposure on window layer characteristics were examined. Unprotected bi-layers from IEC, NREL, and GSE were exposed to damp heat at 85 °C and 85% relative humidity for varying lengths of time at GSE. Sheet resistance and transmission were measured periodically. Samples from IEC were i-ZnO/ITO on soda-lime or 7059 glass. Samples from NREL were i-ZnO/ZnO:Al on soda-lime or 7059 glass. The GSE specimens represent i-ZnO/ITO on soda-lime glass (SLG). Results are shown in

[9] M. Gloeckler, "Numerical Modeling of CIGS Solar Cells: Definition of the Baseline and Explanation of Superposition Failure", M.S. Thesis, Colorado State University, (2003).

[10] T. Walter et al, *Proceedings of the 13th European PVSEC*, (1995), pg. 1999.

[11] L. Kronik. U. Rau, D. Cahen, "Interface redox engineering of Cu(In,Ga)Se2 based solar cells: oxygen, sodium, and chemical bath effects", *Thin Solid Films*, vol. **361/362**, (2000), pp. 353.
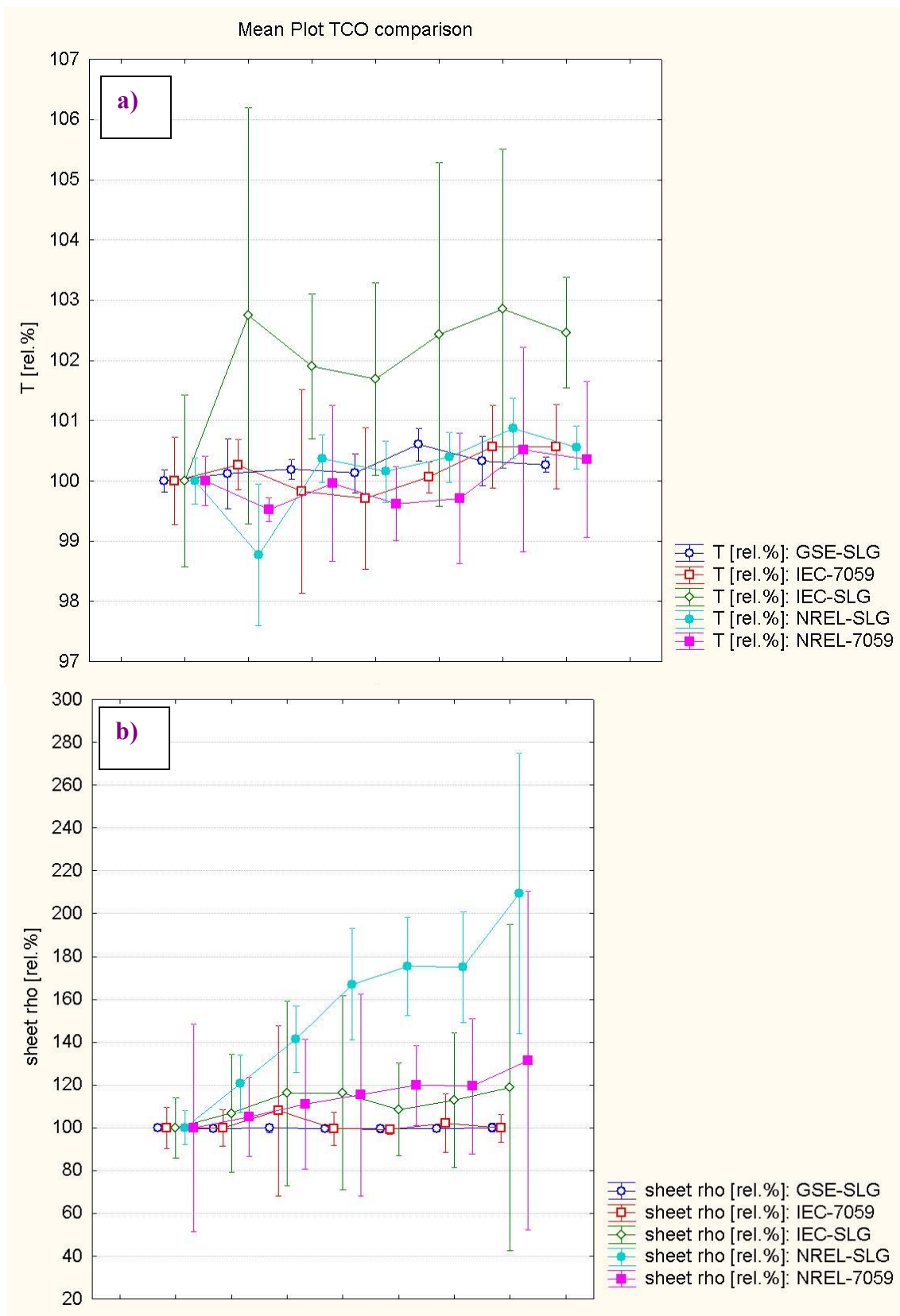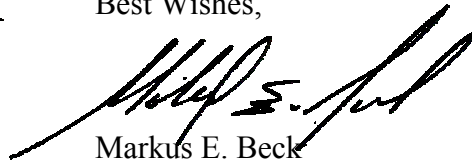
Figure 10: a) Transmission and b) sheet resistance as a function of time for different bi-layers.

Figure 10. As seen in Figure 10a, no changes in transmission above measurement uncertainty are observed. However, several samples exhibited significant changes in sheet resistance, as seen in Figure 10b. Most notably, the NREL bi-layer exhibited about a factor of two increase in sheet resistance on SLG, and about a 30% increase in sheet resistance on 7059. The IEC bi-layer on SLG showed a 20% increase in sheet resistance, whereas the IEC bi-layer on 7059 glass showed no measurable change in resistance. The GSE layers also displayed no measurable change. Error bars in Figure 10 represent 95% confidence intervals for the mean of the sample set. The error bars appear large for some sample sets because the means of those sets are not well-defined, due to small numbers of samples with varying sheet resistances. The large error bars are *not* indicative of larger measurement error or erratic fluctuations in the properties of one sample with time. Thus, for the samples measured, resistance stability depends most strongly on the bi-layer deposition process as well as the TCO material. For samples that degrade, those on SLG degrade more than those on 7059 glass, suggesting that Na may play a role. To this end, the data strengthens the confidence into the GSE window layer with respect to product longevity.

Best Wishes,

Markus E. Beck

Cc: Carolyn Lopez, NREL Subcontract Associate